

Dynamical state of superclusters of galaxies: do superclusters expand or have they started to collapse?

Mirt Gramann and Ivan Suhhonenko

Tartu Observatory, Tõravere 61602, Estonia

3 November 2018

ABSTRACT

We investigate the dynamical state of superclusters in Lambda cold dark matter (Λ CDM) cosmological models, where the density parameter $\Omega_0 = 0.2 - 0.4$ and σ_8 (the rms fluctuation on the $8h^{-1}\text{Mpc}$ scale) is $0.7 - 0.9$. To study the nonlinear regime, we use N-body simulations. We define superclusters as maxima of the density field smoothed on the scale $R = 10h^{-1}\text{Mpc}$. Smaller superclusters defined by the density field smoothed on the scale $R = 5h^{-1}\text{Mpc}$ are also investigated. We find the relations between the radially averaged peculiar velocity and the density contrast in the superclusters for different cosmological models. These relations can be used to estimate the dynamical state of a supercluster on the basis of its density contrast. In the simulations studied, all the superclusters defined with the $10h^{-1}\text{Mpc}$ smoothing are expanding by the present epoch. Only a small fraction of the superclusters defined with $R = 5h^{-1}\text{Mpc}$ has already reached their turnaround radius and these superclusters have started to collapse. In the model with $\Omega_0 = 0.3$ and $\sigma_8 = 0.9$, the number density of objects which have started to collapse is $5 \times 10^{-6}h^3\text{Mpc}^{-3}$.

The results for superclusters in the N-body simulations are compared with the spherical collapse model. We find that the radial peculiar velocities in N-body simulations are systematically smaller than those predicted by the spherical collapse model ($\sim 25\%$ for the $R = 5h^{-1}\text{Mpc}$ superclusters).

Key words: galaxies: clusters: general – cosmology: theory – dark matter – large-scale structure of Universe.

1 INTRODUCTION

Superclusters of galaxies are the largest coherent and massive structures known in the Universe. The existence of superclusters is known since the pioneering studies of Shapley (1930). The nearest example is the Local Supercluster with the Virgo cluster as the central cluster (de Vaucouleurs 1956). The shape, mass and dynamical state of different superclusters have been studied in several papers (see e.g. Einasto et al. 1997; Ettori, Fabian & White 1997; Small et al. 1998; Barmby & Huchra 1998; Batuski et al. 1999; Bardelli et al. 2000; Basilakos, Plionis & Rowan-Robinson 2001; and references therein). Ettori, Fabian & White (1997) studied the mass distribution in the Shapley Supercluster, using X-ray observations. To investigate the dynamical state of the observed overdense regions they used the spherical collapse model (Gunn & Gott 1972; Peebles 1980). Ettori, Fabian & White (1997) found that the core region of the Shapley Supercluster with the radius $6.7h^{-1}\text{Mpc}$ is close to the turnaround point, when the perturbed region ceases to expand and begins to collapse. Bardelli et al. (2000) also analyzed the dynamical state of the Shapley Supercluster,

using the spherical collapse model. They estimated that the total overdensity of galaxies in the Shapley Supercluster is $(N/\bar{N}) \sim 11.3$ on a scale of $10.1h^{-1}\text{Mpc}$ and concluded that, if light traces mass and the density parameter $\Omega = 1$, the Shapley Supercluster has already reached its turnaround radius and has started to collapse. Small et al. (1998) studied the structure and dynamics of the Corona Borealis Supercluster. They found that this supercluster may have started to collapse.

In this paper we study the dynamical state of superclusters in Lambda cold dark matter (Λ CDM) cosmological models, using N-body simulations. These models successfully explain many observations of the large- and small-scale structure including the mass function and the peculiar velocities of clusters of galaxies (see e.g., Ostriker & Steinhardt 1995; Gramann & Hütsi 2001). We study the radial velocity and the density contrast in superclusters. The spherically averaged radial velocity around a system, in the shell of radius R , can be written as

$$u = HR - v, \quad (1)$$

where $v_H = HR$ is the Hubble expansion velocity and v is

the averaged radial peculiar velocity toward the centre of the system. At the turnaround point, the peculiar velocity $v = HR$ and $u = 0$. If $v < HR$, the system expands and if $v > HR$, the system begins to collapse. In the spherical collapse model, the peculiar velocity v is directly related to the density contrast δ (see below). We study the relation between v and δ in N-body simulations and compare the results with the spherical collapse model. Can we estimate the dynamical state of the supercluster on the basis of its density contrast?

The velocity field around superclusters and clusters in different N-body simulations has been studied in several papers (Lee, Hoffman & Ftaclas 1986; Villumsen & Davis 1986; Lilje & Lahav 1991; van Haarlem & van de Weygaert 1993; Hanski et al. 2001). Villumsen & Davis (1986) studied the nature of the velocity field around large clusters in $\Omega = 1$ CDM models. They found that the flowfields when averaged over 4π sr fit spherical collapse model relatively well for density contrasts $\delta < 3$, but the mean radial peculiar velocity is systematically low for increasing δ . van Haarlem & van de Weygaert (1994) studied the evolution of the velocity profile around clusters in $\Omega = 1$ CDM models. They found that for different clusters the agreement with the spherical collapse model can be different. There are clusters where the agreement is very good, but often the predictions of the spherical collapse model compare badly with the actual velocity field in N-body simulations (see Fig. 16-17 in their study). Hanski et al. (2001) studied the velocity profile around four clusters in a $\Omega_0 = 0.3$ Λ CDM model. They found that the radially averaged velocity fields around simulated clusters are compatible with the spherical collapse model.

In this paper we study the velocity field for superclusters in flat Λ CDM models with the density parameter $\Omega_0 = 0.2 - 0.4$, the baryon density $\Omega_b h^2 = 0.02$ and the normalized Hubble constant $h = 0.7$. These values are in agreement with measurements of the density parameter (e.g. Bahcall et al. 1999), with measurements of the baryon density from abundances of light elements (O'Meara et al. 2001; Tytler et al. 2000) and with measurements of the Hubble constant using various distance indicators (Freedman et al. 2001; see also Parodi et al. 2000). To restore the spatial flatness in the low-density models, we assume a contribution from the cosmological constant $\Omega_\Lambda = 1 - \Omega_0$. We also assume that the initial density fluctuation field is a Gaussian density field. In this case, the power spectrum provides a complete statistical description of the field.

We define superclusters as maxima of the density field smoothed on the scale $R = 10h^{-1}\text{Mpc}$. Smaller superclusters in the density field smoothed on the scale $R = 5h^{-1}\text{Mpc}$ are also investigated. We study the number density of superclusters, where the radially averaged peculiar velocity is larger than a given value, $n(>v)$. In particular, we investigate the number density of superclusters which have radially averaged peculiar velocities $v > HR$.

This paper is organized as follows. In Section 2 we consider the spherical collapse model in a flat universe with cosmological constant. We find the relation between the peculiar velocity and the density contrast for the values of the density parameter $\Omega_0 = 0.2 - 0.4$. In Section 3 we describe the N-body simulations and the algorithms that have been used to identify the superclusters. In Section 4 we investigate the density contrast and the radial peculiar velocity for

the superclusters in the N-body simulations and compare the results with the spherical collapse model. The function $n(>v)$ is analyzed in Section 5 and a summary is presented in Section 6.

2 THE SPHERICAL COLLAPSE MODEL

The spherical collapse model describes the evolution of a spherically symmetric perturbation in an expanding universe. Under the assumption of sphericity, the nonlinear dynamics of a collapsing shell is determined by the mass interior to it. The spherical collapse model has been discussed in detail by Tolman (1934), Bondi (1947), Gunn & Gott (1972), Silk (1974, 1977), Peebles (1980) and Schechter (1980). This model has been used in the Press-Schechter (Press & Schechter 1974) formalism to evaluate the mass function of collapsed objects in the universe, as well as to determine the density parameter of the universe from the infalling flow (e.g. Davis & Huchra 1982). In recent years, the spherical collapse model has been used to study the dynamical state of superclusters of galaxies (Ettori, Fabian & White 1997; Small et al. 1998; Bardelli et al. 2000).

Although the Zel'dovich approximation (Zel'dovich 1970) generically yields pancakes and numerical simulations show that many collapsing regions are filamentary (e.g. Gramann 1988; Bertchinger & Gelb 1991), the spherical collapse model has been popular because of its simplicity. Despite its idealized nature, the spherical model appears to give a reasonable description of collapse of high peaks in a random Gaussian density field (Bernardeau 1994). Eisenstein & Loeb (1995) studied an analytical model for the triaxial collapse of cosmological perturbations. They found that the turn-around times of the short axes of a triaxial perturbation are fairly well predicted by the turn-around time of a spherical perturbation with the same initial density.

We consider the spherical collapse model in a flat universe with a cosmological constant, Λ . This model was studied by Peebles (1984), Lahav et al. (1991), Eke, Cole & Frenk (1996) and Lokas & Hoffman (2001). In the spherical collapse model, the mass shell with a radius $R(t)$ contains a fixed mass m and its dynamics satisfies the energy equation

$$\left(\frac{dR}{dt}\right)^2 = \frac{2Gm}{R} + \frac{\Lambda R^2}{3} - K. \quad (2)$$

The constant K is positive for a growing mass perturbation. In a flat universe, the evolution of a scale factor is described by

$$\left(\frac{1}{a} \frac{da}{dt}\right)^2 = \frac{8}{3}\pi G\rho_b + \frac{\Lambda}{3}, \quad (3)$$

where ρ_b is the mean background density. Using eq. (3) we can write eq. (2) as (Peebles 1984)

$$\left(\frac{dR}{da}\right)^2 = \frac{a}{R} \frac{(\omega R^3 - \kappa R + 1)}{(\omega a^3 + 1)}, \quad (4)$$

where κ is a new constant, the present value of a is $a_0 = 1$ and

$$\omega = \frac{1}{\Omega_0} - 1. \quad (5)$$

The density contrast can be expressed as

$$\delta = \frac{a^3}{R^3} - 1. \quad (6)$$

The radial velocity in units of the Hubble velocity is

$$\frac{u}{HR} = \frac{a}{R} \frac{dR}{da} = 1 - \frac{v}{HR}, \quad (7)$$

where v is the peculiar velocity toward the centre of the system.

The perturbed region will turn around when

$$\omega R^3 - \kappa R + 1 = 0. \quad (8)$$

Solving this cubic equation and requiring that a physically sensible root exists, we find that the smallest perturbation which will collapse has

$$\kappa_{\min} = \frac{3\omega^{\frac{1}{3}}}{2^{\frac{2}{3}}}. \quad (9)$$

The corresponding turnaround radius is

$$R_{\text{ta,max}} = (2\omega)^{-\frac{1}{3}}. \quad (10)$$

Perturbations with larger value of κ turn around and collapse earlier. Solving the cubic eq. (8) we can find the turnaround radius R_{ta} as a function of the density parameter ω and constant κ . The solution can be expressed as (Eke, Cole & Frenk 1996)

$$R_{\text{ta}} = -2s^{\frac{1}{3}} \cos\left(\frac{\theta}{3} - \frac{2\pi}{3}\right), \quad (11)$$

where

$$s = \left(\frac{3}{2}\right)^3 \left(\frac{\kappa}{\kappa_{\min}^3}\right)^{\frac{3}{2}} \quad (12)$$

and θ satisfies

$$\cos\theta = \left(\frac{\kappa_{\min}}{\kappa}\right)^{\frac{3}{2}} \quad (0 < \theta < \frac{\pi}{2}). \quad (13)$$

In the limit where $a \ll 1$, we find that

$$\left(\frac{a}{R} \frac{dR}{da}\right)^2 = \frac{a^3}{R^3} (1 - \kappa R) = 1 + \delta - \kappa a \quad (14)$$

and therefore, the density contrast can be written as

$$\delta = -2 \left(\frac{v}{HR}\right) + \kappa a. \quad (15)$$

In linear perturbation theory the peculiar velocity for a spherical mass concentration is determined as

$$\frac{v}{HR} = \frac{1}{3} f(\Omega) \delta, \quad (16)$$

where $f(\Omega)$ is the dimensionless growth factor. For $a \ll 1$, $f(\Omega) = 1$. By using the relation (16), we find from eq.(15) that

$$\delta = \frac{3\kappa}{5} a. \quad (17)$$

In the limit where $a \ll 1$, the density contrast is directly related to the constant κ .

Fig.1 shows the relation between the peculiar velocity in units of the Hubble velocity, v/HR , and the density contrast δ for the flat models at the present moment. We integrated eq. (4) and found the present density contrast and peculiar velocity from eq. (6) and (7), respectively. For each value of

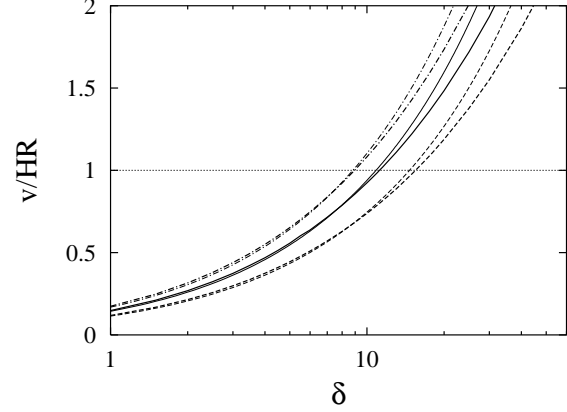


Figure 1. Spherical collapse model. The peculiar velocity in units of the Hubble velocity, v/HR , as a function of the density contrast, δ , in flat universes with the density parameter $\Omega_0 = 0.2$ (dashed lines), $\Omega_0 = 0.3$ (solid lines) and $\Omega_0 = 0.4$ (dot-dashed lines). Heavy lines show the exact solutions obtained by integrating eq. (4) and light lines represent the approximations given by eq. (18).

the initial density contrast δ_i at $a_i \ll 1$, the initial radius R_i was calculated using eq. (6) and the constant κ was determined using eq. (17). For comparison, we show the peculiar velocity given by the approximation derived by Yahil (1985),

$$\frac{v}{HR} = \frac{1}{3} f(\Omega_0) \delta (1 + \delta)^{-\frac{1}{4}}. \quad (18)$$

The growth factor $f(\Omega_0)$ is 0.41, 0.51 and 0.60 for the flat models with $\Omega_0 = 0.2, 0.3$ and 0.4 , respectively. Fig. 1 shows that the approximation (18) agrees well with the numerical solution for the density contrast $\delta < 10$. For larger values of δ , this approximation overestimates the peculiar velocity.

Consider the density contrast at the turnaround point, δ_{ta} , where $v = HR$. We found that $\delta_{\text{ta}} = 15.48, 11.19$ and 8.95 in the flat models with $\Omega_0 = 0.2, 0.3$ and 0.4 , respectively. For comparison, we calculated also the turnaround density contrast for the corresponding open models. The turnaround density contrast in the open models can be expressed as (Regös & Geller 1989)

$$\delta_{\text{ta}} = \left(\frac{\pi}{x_1 - \ln x_2}\right)^2 \omega^3 - 1, \quad (19)$$

where $x_1^2 = (2\Omega_0^{-1} - 1)^2 - 1$ and $x_2 = x_1 + 2\Omega_0^{-1} - 1$. We found that $\delta_{\text{ta}} = 16.22, 11.57$ and 9.17 for the open models with $\Omega_0 = 0.2, 0.3$ and 0.4 , respectively. For the same value of Ω_0 , the turnaround density in the open model is somewhat higher than in the flat model. However, the effect of cosmological constant on δ_{ta} is small.

Next we study the relation between the radial peculiar velocity and density contrast for superclusters in N-body simulations.

3 NUMERICAL MODELS

3.1 Simulations

First, we studied superclusters in a N-body simulation carried out by the Virgo consortium for the flat Λ CDM model

Table 1. N-body simulations with $\Omega_0 = 0.3$ and $\sigma_8 = 0.9$. The power spectrum used is given in eq. (20). In these simulations we studied superclusters in the density field smoothed on the scale $R = 5h^{-1}\text{Mpc}$.

Model	code	N_p	L ($h^{-1}\text{Mpc}$)	N_s	$N_{0.5}$	N_c
M1	AP ³ M	256 ³	239.5	1414	342	63
M2	PM	256 ³	239.5	1374	259	23
M3	PM	128 ³	192	662	153	14

with a cosmological constant. The Virgo simulations are described in detail by Jenkins et al. (1998). These simulations were created using an adaptive particle-particle/particle-mesh (AP³M) code as described by Couchman, Thomas & Pearce (1995) and Pearce & Couchman (1997). In the $\Omega_0 = 0.3$ Λ CDM model studied here, the power spectrum of the initial conditions was chosen to be in the form given by Bond & Efstathiou (1984),

$$P(k) = \frac{Ak}{[1 + (aq + (bq)^{3/2} + (cq)^2)^\nu]^{2/\nu}}, \quad (20)$$

where $q = k/\Gamma$, $a = 6.4h^{-1}\text{Mpc}$, $b = 3h^{-1}\text{Mpc}$, $c = 1.7h^{-1}\text{Mpc}$, $\nu = 1.13$ and $\Gamma = \Omega_0 h = 0.21$. The normalization constant, A , was chosen by fixing the value of σ_8 (the linearly extrapolated mass fluctuation in spheres of radius $8h^{-1}\text{Mpc}$) to be 0.9. The evolution of particles was followed in the comoving box of size $L = 239.5h^{-1}\text{Mpc}$. The number of particles was $N_p = 256^3$. Therefore, the mean particle separation $\lambda_p = L/N_p^{1/3} = 0.9355h^{-1}\text{Mpc}$. We denote this Λ CDM model as the model M1.

We also investigated superclusters in a series of N-body simulations we carried out for flat Λ CDM models, where the density parameter $\Omega_0 = 0.2-0.4$ and $\sigma_8 = 0.7-0.9$. In these simulations, the evolution of particles was followed by using a particle-mesh (PM) code described by Gramann (1988) and Suhhonenko & Gramann (1999). The PM method is discussed in detail by Hockney & Eastwood (1981) and Efstathiou et al. (1985). We used the PM code, where the number of cells was the same as the number of particles. We denote these flat Λ CDM models as the models M2-M3, S1-S4 and L1-L4.

In the models M2 and M3, the cosmological parameters were chosen similar to the model M1. We chose the flat $\Omega_0 = 0.3$, $\Omega_\Lambda = 0.7$ model and used the initial power spectrum $P(k)$ given in eq. (20) (with $\sigma_8 = 0.9$). In the model M2, we followed the evolution of 256³ particles in the box of size $L = 239.5h^{-1}\text{Mpc}$. In the model M3, the number of particles was $N_p = 128^3$ and the box size $L = 192h^{-1}\text{Mpc}$. Table 1 lists the code, the number of particles and the box size used in models M1, M2 and M3, respectively. Suhhonenko & Gramann (2002) used the models M1 and M2 to investigate the rms peculiar velocity of galaxy clusters for different cluster masses and radii.

In the models S1-S4 and L1-L4, the number of particles was $N_p = 128^3$. In these models, the initial power spectrum was calculated by using the fast Boltzmann code CMBFAST developed by Seljak & Zaldarriaga (1996). The normalized Hubble constant was chosen to be $h = 0.7$ and the baryon density $\Omega_b h^2 = 0.02$. Table 2 lists the density parameter Ω_0 , σ_8 and the box size L used in the models S1-S4 and L1-

Table 2. N-body simulations, where the evolution of 128³ particles was followed by the PM code. The power spectrum of the initial density field was calculated by using the code CMBFAST. In the models S1-S4, we studied superclusters in the density field smoothed on the scale $R = 5h^{-1}\text{Mpc}$. In the models L1-L4, we used the smoothing scale $R = 10h^{-1}\text{Mpc}$.

Model	Ω_0	σ_8	L ($h^{-1}\text{Mpc}$)	N_s	$N_{0.5}$	N_c
S1	0.2	0.8	192	541	80	4
S2	0.3	0.7	192	633	119	11
S3	0.3	0.9	192	630	149	20
S4	0.4	0.8	192	699	191	25
L1	0.2	0.8	384	606	20	—
L2	0.3	0.7	384	611	14	—
L3	0.3	0.9	384	687	57	—
L4	0.4	0.8	384	718	52	—

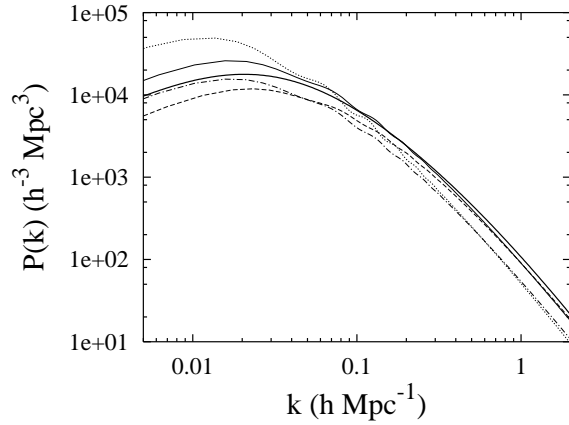


Figure 2. Power spectra used in the N-body simulations. The heavy solid line shows the power spectrum given in eq. (20) for $\Omega_0 = 0.3$ and $\sigma_8 = 0.9$. The light curves show the power spectra calculated by using the code CMBFAST. The dotted line shows the power spectrum for $\Omega_0 = 0.2$, $\sigma_8 = 0.8$, the solid line for $\Omega_0 = 0.3$, $\sigma_8 = 0.9$, the dot-dashed line for $\Omega_0 = 0.3$, $\sigma_8 = 0.7$ and the dashed line for $\Omega_0 = 0.4$, $\sigma_8 = 0.8$. The normalized Hubble constant $h = 0.7$.

L4. We studied the flat models with a cosmological constant $\Omega_\Lambda = 1 - \Omega_0$.

For the models M3 and S3, all the parameters are the same, except of the form of the initial power spectrum. In the model M3, we used the approximation given in eq. (20) and in the model S3, the power spectrum was calculated numerically by using the code CMBFAST.

Fig. 2 shows the power spectra used in the N-body simulations for different values of the parameters Ω_0 and σ_8 . The light curves show the numerical power spectra calculated by using the code CMBFAST. In the models studied, the power spectrum on large scales is quite different. For the same value of σ_8 , the amplitude of the large-scale density fluctuations is highest for $\Omega_0 = 0.2$ and lowest for $\Omega_0 = 0.4$. The light solid line shows the power spectrum for $\Omega_0 = 0.3$ and $\sigma_8 = 0.9$. For comparison, we show the power spectrum given in eq. (20) for $\Omega_0 = 0.3$ and $\sigma_8 = 0.9$ (heavy solid line). We see that on large scales, the numerical power spectrum

is considerably higher than the power spectrum given in eq. (20) ($\sim 26\%$ at the wavelength $\lambda = 2\pi/k = 192h^{-1}\text{Mpc}$).

3.2 Selection of superclusters

To select the superclusters in the N-body simulations, we used the following method:

(1) We calculated the density contrast on a grid. For each grid point, the density contrast was determined as

$$\delta = \frac{N}{\bar{N}} - 1, \quad (21)$$

where N is the number of particles in the sphere of radius R around the grid point, and

$$\bar{N} = \frac{4\pi}{3} \frac{N_p R^3}{L^3} \quad (22)$$

is the mean number of particles in the sphere of radius R . We denote the number of cells in the grid as N_g^3 .

(2) We found the density maxima on the grid. The grid point was considered as a density maximum, if its density contrast was higher than the density contrast in all neighbouring grid points. In the following, we studied the density maxima, where the density contrast was $\delta > 1$.

(3) We identified the candidate supercluster centres. For each grid point, where the density maximum was determined, we found all particles in a cube with the size $l = L/N_g$ around this grid point. For each particle we calculated the density contrast using eq. (21), where N was the number of particles in the sphere of radius R around this fixed particle. The location of the particle, where the density contrast had the maximum value, was identified as the candidate supercluster centre.

(4) The final supercluster list was obtained by deleting the candidate superclusters with lower density contrast in all pairs separated by less than the radius R .

In this way we define the superclusters as maxima of the density field smoothed with a top-hat window with radius R . In the models M1-M3 and S1-S4, we used the smoothing radius $R = 5h^{-1}\text{Mpc}$. In the models M1 and M2, the mean number of particles in spheres of $R = 5h^{-1}\text{Mpc}$ is $\bar{N} = 639.4$, in the models M3 and S1-S4 - $\bar{N} = 155.1$. To select superclusters for the models M1 and M2, we used a 80^3 grid. In this case, the cell size was $l = L/N_g = 2.99h^{-1}\text{Mpc}$. To identify superclusters for the models M3 and S1-S4, we used a 64^3 grid ($l = 3h^{-1}\text{Mpc}$). In the models L1-L4, we studied the superclusters defined with $R = 10h^{-1}\text{Mpc}$. In these models, the mean number of particles in spheres of $R = 10h^{-1}\text{Mpc}$ is $\bar{N} = 155.1$. To select superclusters, we used a 64^3 grid ($l = 6h^{-1}\text{Mpc}$).

4 RADIAL VELOCITY AND DENSITY CONTRAST IN THE SUPERCLUSTERS

Table 1 and Table 2 show the number of superclusters, N_s , identified in different models. For each supercluster, we investigated the density contrast, δ , and the radially averaged peculiar velocity, v . The density contrast in a supercluster was determined as

$$\delta = \frac{N_f}{\bar{N}} - 1, \quad (23)$$

where N_f is the number of particles in the sphere of radius R around the centre of the supercluster. The radially averaged peculiar velocity for the supercluster, in a shell of radius R , was defined as

$$v = -\frac{1}{N_l} \sum_{i=1}^{N_l} (\vec{v}_i' - \vec{v}_0') \cdot \hat{r}_i, \quad (24)$$

where N_l is the number of particles in the shell $0.1R$ wide, \vec{v}_i' is the peculiar velocity of the particle i at a radial distance \vec{r}_i from the centre of the supercluster, \hat{r}_i is the unit vector in the direction of the particle i and \vec{v}_0' is the mean peculiar velocity of all the particles within the sphere of radius R ,

$$\vec{v}_0' = \frac{1}{N_f} \sum_{i=1}^{N_f} \vec{v}_i'. \quad (25)$$

Fig. 3 shows the averaged radial peculiar velocity of a supercluster in units of the Hubble velocity, v/HR , vs. the density contrast of the supercluster in the models M1, M2 and M3. The superclusters were defined with $R = 5h^{-1}\text{Mpc}$. In the models M1, M2 and M3, the number of superclusters is 1414, 1374 and 662, respectively. We see a close correlation between the peculiar velocity and the density contrast of a supercluster. We can estimate the dynamical state of the supercluster on the basis of its density contrast.

For comparison, we also show in Fig. 3 the peculiar velocity predicted in the flat spherical collapse model for $\Omega_0 = 0.3$. The radially averaged peculiar velocity of superclusters is systematically smaller than that predicted by the spherical collapse model.

We investigated the mean peculiar velocity and the standard deviation for the superclusters in different density intervals. The superclusters were divided into subgroups according to their density contrast. We studied the velocities in fifteen subgroups, where the logarithm of the density contrast was in the range $\log \delta = 0 - 0.1, 0.1 - 0.2, \dots, 1.4 - 1.5$. The mean peculiar velocity and standard deviation were determined for the intervals which contained at least eight superclusters. The lower right panel in Fig. 3 shows the mean peculiar velocity determined in the models M1, M2 and M3. The error bars show the standard deviation. For clarity, the standard deviation is only shown for the model M3. In the models M1, M2 and M3, the standard deviation is similar.

The models M1 and M2 differ from each other by the code used to follow the evolution of particles. The model M1 was created using a AP³M code and the model M2 by using a PM code. Fig. 3 shows that in the model M1, the mean peculiar velocities are somewhat higher than in the model M2. For example, in the range $\delta = 10.0 - 12.6$, the mean peculiar velocities are $\bar{v} = 0.78HR$ and $\bar{v} = 0.68HR$ in the models M1 and M2, respectively. This difference is probably due to the smoothing inherent to the PM method. However, the effect of the code on the mean peculiar velocity is not large ($\sim 15\%$ in the range $\delta = 10.0 - 12.6$).

In the model M3, the box size L and the number of particles, N_p , are smaller than in the models M1 and M2. In this model for $R = 5h^{-1}\text{Mpc}$, the box size $L = 38.4R$ and the mean particle separation $\lambda_p = 0.3R$. The same values for L/R and λ_p/R are used in the models S1-S4 and L1-L4. Fig. 3 shows that the mean peculiar velocities in the model M3 are similar to the mean velocities in the models M1 and

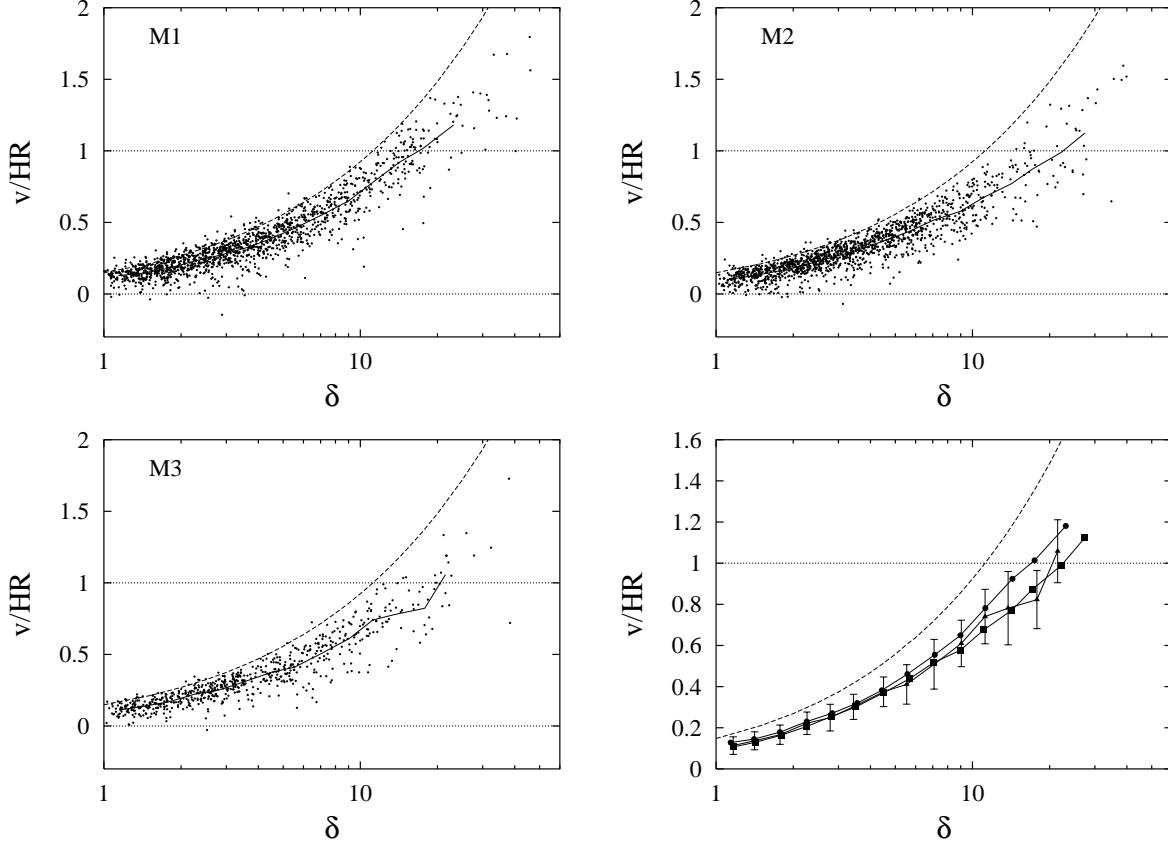


Figure 3. The averaged radial peculiar velocity of a supercluster in units of the Hubble velocity, v/HR , vs. the density contrast of the supercluster in the models M1 (upper right panel), M2 (upper left panel) and M3 (lower left panel). The solid lines show the mean peculiar velocity for the superclusters. For comparison, we show the peculiar velocity in the spherical collapse model for $\Omega_0 = 0.3$ (dashed lines). The lower right panel shows the mean peculiar velocity in the models M1 (circles), M2 (squares) and M3 (triangles). The error bars show the standard deviation. For clarity, error bars are only shown for the model M3. The superclusters are defined with $R = 5h^{-1}\text{Mpc}$.

M2. For example, in the range $\delta = 10 - 12.6$, the mean peculiar velocity is $\bar{v} = 0.74HR$. Therefore, a box size $L = 38.4R$ and a mean particle separation $\lambda_p = 0.3R$ are sufficient to study the mean peculiar velocities in superclusters defined with radius R .

We can compare the mean peculiar velocities of superclusters with the predictions of the spherical collapse model. Lets consider the model M1. In this model, for the range $\delta = 1.00 - 1.26$, the mean density contrast is 1.14 and the mean peculiar velocity is $\bar{v} = 0.13HR$. For comparison, in the spherical collapse model, the peculiar velocity for $\delta = 1.14$ is $v = 0.17HR$. For the range $\delta = 10.0 - 12.6$, the mean density contrast for superclusters is 11.2 and $\bar{v} = 0.78HR$. In the spherical collapse model, the peculiar velocity for $\delta = 11.2$ is $v = 1.0HR$. Therefore, the mean peculiar velocities in the simulation are $\sim 25\%$ smaller than those predicted by the spherical collapse model. The difference in the peculiar velocities for $\delta \approx 1$ and $\delta \approx 10$ is similar. In the model M2 and M3, the deviations from the spherical collapse model are somewhat larger than in the model M1 ($\sim 35\%$ and $\sim 30\%$ for the model M2 and M3, respectively).

Fig. 4 shows the radially averaged peculiar velocities for the superclusters in the models S1-S4. The mean peculiar velocity with a standard deviation is determined similarly as in the models M1-M3. Panel (a) shows the peculiar velocities

for the model S1 ($\Omega_0 = 0.2$) and S4 ($\Omega_0 = 0.4$). For the same value of the density contrast, the mean peculiar velocity is larger, if the density parameter Ω_0 is larger. For the range $\delta = 5.0 - 6.3$, the peculiar velocity $v/HR = 0.37 \pm 0.08$ and $v/HR = 0.52 \pm 0.11$ in the model S1 and S4, respectively. For the range $\delta = 10 - 12.6$, the peculiar velocity $v/HR = 0.62 \pm 0.08$ and $v/HR = 0.87 \pm 0.10$, respectively.

Panel (b) in Fig. 4 shows the peculiar velocities for the superclusters in the model S2 and S3. In these models $\Omega_0 = 0.3$. In the model S2, the parameter $\sigma_8 = 0.7$ and in the model S3, the $\sigma_8 = 0.9$. We see that the mean peculiar velocities in the model S3 are somewhat smaller than the peculiar velocities in the model S2. The difference between the models S2 and S3 is not large. For the range $\delta = 5.0 - 6.3$, the peculiar velocity $v/HR = 0.48 \pm 0.07$ and $v/HR = 0.43 \pm 0.10$ in the model S2 and S3, respectively. For the range $\delta = 10 - 12.6$, the peculiar velocity $v/HR = 0.77 \pm 0.14$ and $v/HR = 0.73 \pm 0.12$, respectively. The peculiar velocities in the model S3 are similar to the peculiar velocities in the model M3.

We compared the mean peculiar velocities for the superclusters in the models S1-S4 with the predictions of the spherical collapse model. The mean peculiar velocities in the models S1, S2 and S4 are $\sim 25\%$ smaller than those predicted by the spherical collapse model. In the model S3, the

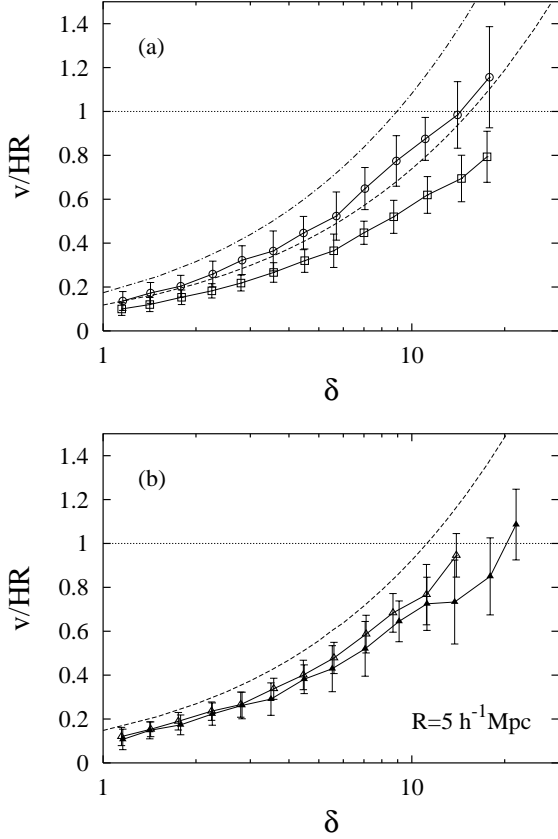


Figure 4. The radially averaged peculiar velocity for the superclusters in the models S1-S4. The superclusters are defined in the density field smoothed on the scale $R = 5h^{-1}\text{Mpc}$. Panel (a) shows the peculiar velocities for the model S1 (squares) and S4 (circles). For comparison, we show the peculiar velocities predicted by the spherical collapse model for $\Omega_0 = 0.2$ (dashed line) and for $\Omega_0 = 0.4$ (dot-dashed line). Panel (b) shows the peculiar velocities for the model S2 (open triangles) and S3 (filled triangles). The dashed line describes the peculiar velocities in the spherical collapse model for $\Omega_0 = 0.3$.

difference is $\sim 30\%$. In all models, this difference is similar for different values of the density contrast.

We also determined the turnaround density contrast δ_{ta} for the $R = 5h^{-1}\text{Mpc}$ superclusters. We found all the superclusters, where the peculiar velocity in units of the Hubble velocity, v/HR , is in the range $[0.9, 1.1]$ and calculated the mean density contrast and the standard deviation for these superclusters. Table 3 shows the density contrast δ_{ta} for the models studied. For the model M1, we found that $\delta_{\text{ta}} = 16.2 \pm 4.6$. For comparison, in the spherical collapse model the turnaround density contrast is 11.19 for $\Omega_0 = 0.3$ (see Section 2). For the model S1 and S4, we found that $\delta_{\text{ta}} = 23.7 \pm 7.1$ and $\delta_{\text{ta}} = 12.3 \pm 2.2$, respectively. In the spherical model, $\delta_{\text{ta}} = 15.48$ and 8.95 for $\Omega_0 = 0.2$ and $\Omega_0 = 0.4$, respectively. The turnaround density contrast for the superclusters in N-body simulations is substantially larger than the turnaround density contrast in the spherical collapse model.

We also studied superclusters in the models L1-L4. In these models the box size was $L = 384h^{-1}\text{Mpc}$ and we investigated the superclusters in the density field smoothed on

Table 3. The turnaround density contrast, δ_{ta} , for the superclusters studied with $R = 5h^{-1}\text{Mpc}$.

Model	δ_{ta}
M1	16.2 ± 4.6
M2	18.1 ± 4.3
M3	16.8 ± 3.6
S1	23.7 ± 7.1
S2	14.6 ± 1.8
S3	18.2 ± 4.0
S4	12.3 ± 2.2

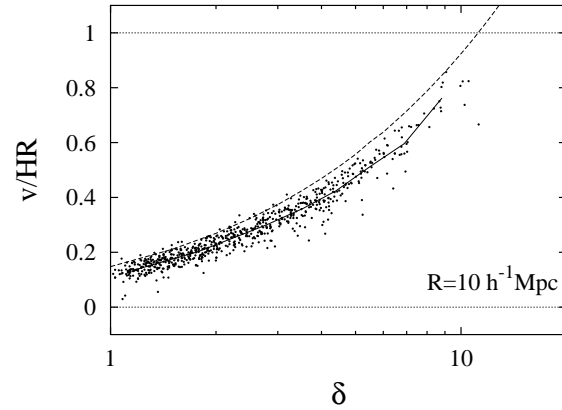


Figure 5. The radially averaged peculiar velocity for 687 superclusters of the model L3. The superclusters are defined with $R = 10h^{-1}\text{Mpc}$. The solid line shows the mean peculiar velocity for the superclusters and the dashed line describes the peculiar velocity in the spherical collapse model for $\Omega_0 = 0.3$.

the scale $R = 10h^{-1}\text{Mpc}$. Fig. 5 shows the radially averaged peculiar velocity of a supercluster in units of the Hubble velocity, v/HR , vs. the density contrast of the supercluster, for 687 superclusters of the model L3. For comparison, we show the peculiar velocities predicted in the spherical collapse model for $\Omega_0 = 0.3$. We see that also for the superclusters studied with $10h^{-1}\text{Mpc}$ smoothing, the mean infall velocities are systematically smaller than those predicted by the spherical collapse model.

Fig. 6 shows the peculiar velocities for the superclusters in the models L1-L4. For comparison, the dotted line in panel (b) shows the peculiar velocities for the $R = 5h^{-1}\text{Mpc}$ superclusters in the model M1. For the $R = 10h^{-1}\text{Mpc}$ superclusters, the mean peculiar velocities in units of the Hubble velocity, \bar{v}/HR , are somewhat higher than for the $R = 5h^{-1}\text{Mpc}$ superclusters. For the range $\delta = 5.0 - 6.3$, the peculiar velocity $v/HR = 0.43 \pm 0.04$ and $v/HR = 0.63 \pm 0.06$ in the model L1 and L4, respectively. The peculiar velocity $v/HR = 0.54 \pm 0.04$ and $v/HR = 0.51 \pm 0.05$, in the model L2 and L3, respectively. The mean peculiar velocities for the superclusters in the models L1-L4 are $\sim 15\%$ smaller than those predicted by the spherical collapse model.

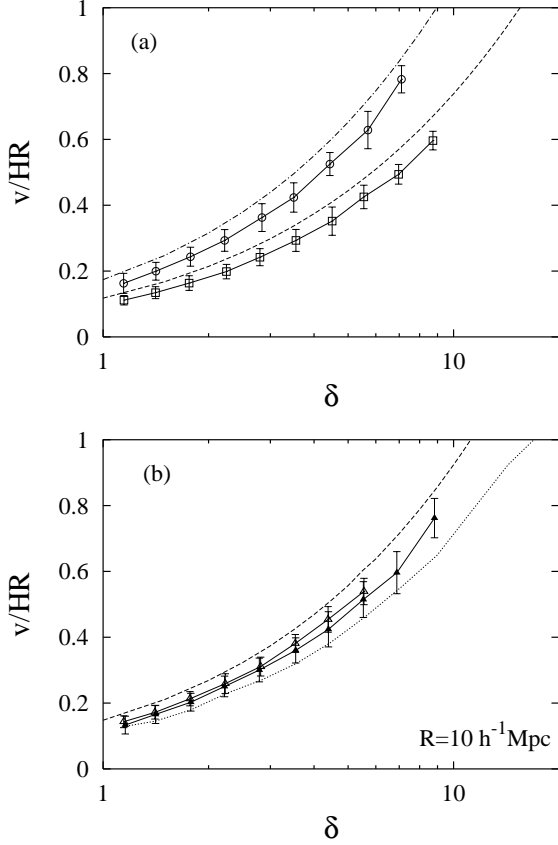


Figure 6. The peculiar velocity for the superclusters in the models L1-L4. Panel (a) shows the peculiar velocities for the model L1 (squares) and L4 (circles). For comparison, we show the peculiar velocities predicted by the spherical collapse model for $\Omega_0 = 0.2$ (dashed line) and for $\Omega_0 = 0.4$ (dot-dashed line). Panel (b) shows the peculiar velocities for the model L2 (open triangles) and L3 (filled triangles). The dotted line shows the mean peculiar velocity for the $R = 5h^{-1}\text{Mpc}$ superclusters in the model M1 and the dashed line describes the peculiar velocities in the spherical collapse model for $\Omega_0 = 0.3$.

5 VELOCITY DISTRIBUTION FOR THE SUPERCLUSTERS

We investigated the number of superclusters, where the radially averaged peculiar velocity is larger than a given value, $N(>v)$. We denote the number of superclusters, which have peculiar velocities $v > HR$ and, therefore, have already started to collapse, as N_c . We also examined the number of superclusters, which have peculiar velocities $v > 0.5HR$. We denote this number as $N_{0.5}$. Table 1 and Table 2 show the numbers N_c and $N_{0.5}$ for the different models studied. In the model M1, we found 63 superclusters which have already started to collapse.

Panel (a) in Fig. 7 shows the number density of superclusters, where the radially averaged peculiar velocity is larger than a given value, $n(>v)$. The number density is given for the superclusters in the models M1-M3. The function $n(>v)$ was determined as

$$n(>v) = \frac{N(>v)}{L^3}. \quad (26)$$

We also show the Poisson error bars for the number density.

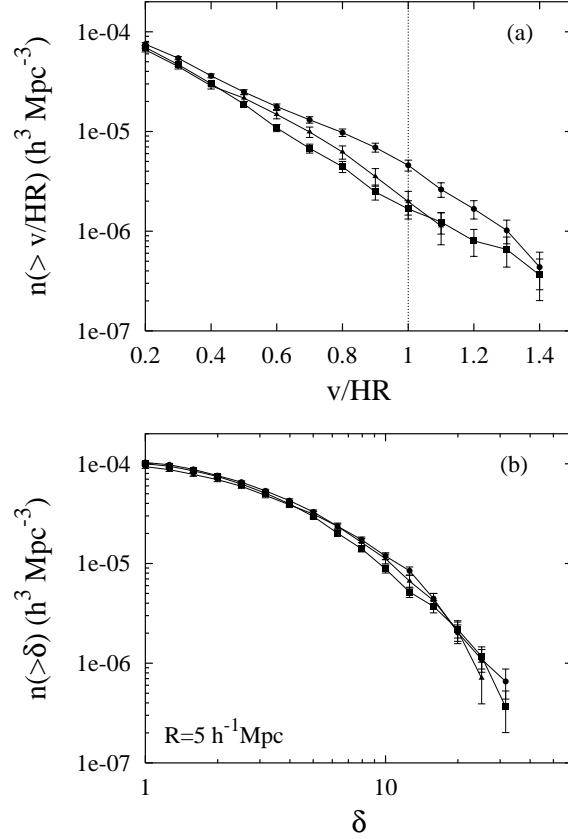


Figure 7. (a) The number density of superclusters, where the radially averaged peculiar velocity is larger than a given value, $n(>v)$. The number density is shown for the superclusters in the model M1 (circles), M2 (squares) and M3 (triangles). (b) The number density of superclusters, where the density contrast is larger than a given value, $n(>\delta)$. The density distribution is given for the same models as in panel a. Error bars in panels a and b denote Poisson errors.

Panel (b) in Fig. 7 demonstrates the density distribution for the superclusters in the models M1-M3. The density distribution in these models is similar, but the velocity distribution is different. The function $n(>v)$ for the model M1 is higher than for the model M2. In the model M1 and M2, the number density of superclusters that have peculiar velocities $v > HR$, is $4.6 \times 10^{-6} h^3 \text{Mpc}^{-3}$ and $1.7 \times 10^{-6} h^3 \text{Mpc}^{-3}$, respectively. The difference between the models M1 and M2 is smaller for smaller peculiar velocities. The velocity distribution in the model M3 is similar to the model M2. Therefore, the number density $n(>v)$ in the model M3 is probably underestimated.

Fig. 8 shows the number density, $n(>v)$, for the superclusters in the models S1-S4 and L1-L4. We can use models S1-S4 and L1-L4 to estimate the lower limit for the function $n(>v)$ in different models. Also, we can examine the relative differences between the different models. Panel (a) in Fig. 8 shows the number density for the $R = 5h^{-1}\text{Mpc}$ superclusters in the models S1-S4 ($L = 192h^{-1}\text{Mpc}$). The function $n(>v)$ is lowest for the model S1 ($\Omega_0 = 0.2$) and highest for the model S4 ($\Omega_0 = 0.4$). In the model S1, we found 4 superclusters, which have started to collapse. In the model S4, this number was 25. The number density of su-

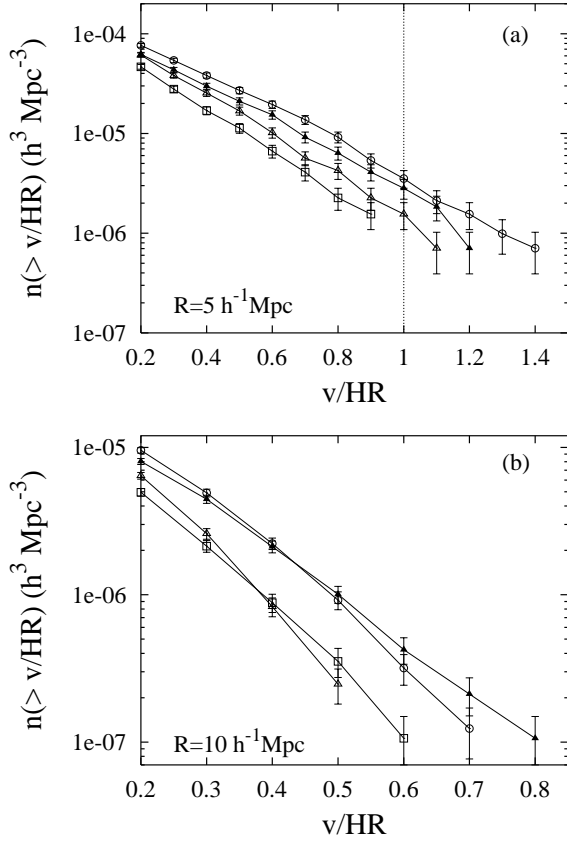


Figure 8. (a) The velocity distribution for the superclusters in the model S1 (squares), S2 (open triangles), S3 (filled triangles) and S4 (circles). (b) The velocity distribution for the superclusters in the model L1 (squares), L2 (open triangles), L3 (filled triangles) and L4 (circles). Error bars in panels a and b denote Poisson errors.

perclusters, which have peculiar velocities $v > 0.5HR$, is $1.1 \times 10^{-5} h^3 \text{Mpc}^{-3}$ and $2.7 \times 10^{-5} h^3 \text{Mpc}^{-3}$, in the model S1 and S4, respectively.

Panel (b) in Fig. 8 shows the number density for the $10h^{-1}\text{Mpc}$ superclusters in the models L1-L4 ($L = 384h^{-1}\text{Mpc}$). The velocity distributions in the models L1 and L2 are similar. In the model L1, the density parameter Ω_0 is smaller, but the amplitude of the large-scale density fluctuations is larger than in model L2 (see Fig. 2). The number density of superclusters, which have peculiar velocities $v > 0.5HR$, is $3.5 \times 10^{-7} h^3 \text{Mpc}^{-3}$ and $2.4 \times 10^{-7} h^3 \text{Mpc}^{-3}$, in the models L1 and L2, respectively. The velocity distributions in the models L3 and L4 are also similar. In the model L4, the density parameter Ω_0 is higher, but the amplitude of the large-scale density fluctuations is smaller than in the model L3. The number density of superclusters, which have peculiar velocities $v > 0.5HR$, is $1.0 \times 10^{-6} h^3 \text{Mpc}^{-3}$ and $0.9 \times 10^{-6} h^3 \text{Mpc}^{-3}$, in the models L3 and L4, respectively.

In the simulations studied, all the superclusters defined with $10h^{-1}\text{Mpc}$ smoothing are expanding by the present epoch. In the models L3 ($\Omega_0 = 0.3$) and L4 ($\Omega_0 = 0.4$), the maximum density contrast for the $R = 10h^{-1}\text{Mpc}$ superclusters is 11.2 and 7.9, respectively. The turnaround density contrast for the $R = 10h^{-1}\text{Mpc}$ superclusters is expected to be similar or somewhat smaller than for the

$R = 5h^{-1}\text{Mpc}$ superclusters (see Fig. 4 and Fig. 6). In the model M1 ($\Omega_0 = 0.3$) and S4 ($\Omega_0 = 0.4$), the turnaround density contrast for the $R = 5h^{-1}\text{Mpc}$ superclusters is $\delta_{ta} = 16.2 \pm 4.6$ and $\delta_{ta} = 12.3 \pm 2.2$, respectively. Therefore, the $R = 10h^{-1}\text{Mpc}$ superclusters in the models L3 and L4 are close to the turnaround point.

6 SUMMARY

In this paper we have investigated the dynamical state of superclusters in flat ΛCDM models. We analyzed superclusters in the Virgo simulation for the ΛCDM model with $\Omega_0 = 0.3$ and $\sigma_8 = 0.9$. This simulation was carried out using the AP³M code. We also investigated superclusters in a series of N-body simulations we carried out for flat ΛCDM models, where the density parameter $\Omega_0 = 0.2 - 0.4$ and $\sigma_8 = 0.7 - 0.9$. In these simulations, a PM code was used. To identify superclusters in simulations we used a method where superclusters were defined as maxima of the density field smoothed on the scale $R = 10h^{-1}\text{Mpc}$. Smaller superclusters in the density field smoothed on the scale $R = 5h^{-1}\text{Mpc}$ were also examined. For each supercluster identified, we determined the density contrast, δ , and the radially averaged peculiar velocity, v (see eq. (23-24)).

The results for the superclusters in the N-body simulations were compared with the spherical collapse model. We found that the radial peculiar velocities in the N-body simulations are systematically smaller than those predicted by the spherical collapse model ($\sim 15\%$ and $\sim 25\%$ for the $R = 10h^{-1}\text{Mpc}$ and $R = 5h^{-1}\text{Mpc}$ superclusters, respectively). The deviations from the spherical collapse model are similar for $\delta \approx 1$ and $\delta \approx 10$. We also studied the turnaround density contrast for superclusters. We found that the turnaround density contrast for superclusters is substantially larger than that predicted by the spherical collapse model. In the Virgo simulation with $\Omega_0 = 0.3$, the turnaround density contrast is $\delta_{ta} = 16.2 \pm 4.6$ for the $R = 5h^{-1}\text{Mpc}$ superclusters. For comparison, in the spherical model the turnaround density contrast is 11.19 for $\Omega_0 = 0.3$.

We found the relations between δ and v for different cosmological models. These relations can be used to estimate the dynamical state of a supercluster on the basis of its density contrast. The density contrast for superclusters on large scales can be determined from the new large galaxy redshift surveys. The results of our study show how the density contrast is related to the radial peculiar velocity of the supercluster. For example, in the model with $\Omega_0 = 0.3$, $\sigma_8 = 0.9$ and $R = 10h^{-1}\text{Mpc}$, the peculiar velocity $v/HR = 0.54 \pm 0.04$ for the range $\delta = 5.0 - 6.3$. The $v/HR - \delta$ relation for different values of R and σ_8 is similar.

On the other hand, recent improvements of the techniques for measuring distances of galaxies allow compilation of large samples of galaxies with measured peculiar velocities. We can use this information to study the radially averaged peculiar velocity of superclusters. On the basis of this peculiar velocity we can estimate the mass-density contrast in the superclusters and compare it with the galaxy-density contrast. In this way we can study the relation between the mass distribution and the galaxy distribution on large scales.

In the simulations studied, all the superclusters defined

with $10h^{-1}\text{Mpc}$ smoothing have peculiar velocities $v < HR$ and, therefore, are expanding by the present epoch. A small fraction of the $R = 5h^{-1}\text{Mpc}$ superclusters has already reached their turnaround radius and these superclusters have started to collapse. In the Virgo simulation, the number density of superclusters, which have started to collapse, is $4.6 \times 10^{-6} h^3 \text{Mpc}^{-3}$. The $R = 10h^{-1}\text{Mpc}$ superclusters in the models with $\Omega_0 = 0.3$, $\sigma_8 = 0.9$ and $\Omega_0 = 0.4$, $\sigma_8 = 0.8$ are close to the turnaround point.

ACKNOWLEDGEMENTS

We thank J. Einasto, M. Einasto, P. Heinämäki, G. Hütsi, J. Jaaniste and E. Saar for useful discussions. This work has been supported by the ESF grant 3601. The Virgo simulation used in this paper is available at <http://www.mpa-garching.mpg.de/Virgo/virgoproject.html>. This simulation was carried out at the Computer Center of the Max-Planck Society in Garching and at the EPCC in Edinburgh, as part of the Virgo Consortium project. The code CMBFAST used in this paper, is available at <http://arcturus.mit.edu/~matiasz/CMBFAST/cmbfast.html>.

REFERENCES

- Bahcall N.A., Ostriker J.P., Perlmutter S., Steinhardt P.J., 1999, *Science*, 1481
- Bardelli S., Zucca E., Zamorani G., Moscardini L., Scaramella R., 2000, 312, 540
- Barmby P., Huchra J.P., 1998, *AJ*, 115, 6
- Basilakos S., Plionis M., Rowan-Robinson M., 2001, *MNRAS*, 323, 47
- Batuski D.J., Miller C.J., Slinglend K.A., Balkowski C., Maurogordato S., Cayatte V., Felenbok P., Olowin R., 1999, *ApJ*, 520, 491
- Bernardeau F., 1994, *ApJ*, 427, 51
- Bertschinger E., Gelb J.M., 1991, *Comp. Phys.*, 5, 164
- Bond J.R., Efstathiou G., 1984, *ApJ*, 285, L45
- Bondi H., 1947, *MNRAS*, 107, 410
- Couchman H.M.P., Thomas P.A., Pearce F.R., 1995, *ApJ*, 452, 797
- Davis M., Huchra J., 1982, *ApJ*, 254, 437
- de Vaucouleurs G., 1956, *Vistas Astron.*, 2, 1584
- Einasto M., Tago E., Jaaniste J., Einasto J., Andernach H., 1997, *A&AS*, 123, 119
- Eisenstein D.J., Loeb A., 1995, *ApJ*, 439, 520
- Eke V.R., Cole S., Frenk C.S., 1996, *MNRAS*, 282, 263
- Ettori S., Fabian A.C., White D.A., 1997, *MNRAS*, 289, 787
- Freedman W.L. et al., 2001, *ApJ*, 553, 47
- Gramann M., 1988, *MNRAS*, 234, 569
- Gramann M., Hütsi G., 2001, *MNRAS*, 327, 538
- Gunn J.E., Gott J.R., 1972, *ApJ*, 176, 1
- Hanski M.O., Theureau G., Ekholm T., Teerikorpi P., 2001, *A&A*, 378, 345
- Hockney R.W., Eastwood J.W. 1981, *Numerical simulations using particles* (New York: McGraw-Hill)
- Jenkins A. et al. (The Virgo Consortium), 1998, *ApJ*, 499, 20
- Lahav O., Lilje P.B., Primack J.R., Rees M.J., 1991, 251, 128
- Lee H., Hoffman Y., Ftaclos C., 1986, *ApJ*, 304, L11
- Lilje P.B., Lahav O., 1991, *ApJ*, 374, 29
- Lokas E.L., Hoffmann Y., 2001, *Proceedings of the 3rd International Workshop on the Identification of Dark Matter*, ed. N.J.C. Spooner & V. Kudryavtsev, World Scientific, Singapore, p. 121
- O'Meara J.M., Tytler D., Kirkman D., Suzuki N., Prochaska J.X., Lubin D., Wolfe A.M., 2001, *ApJ*, 552, 718
- Ostriker J.P., Steinhardt P.J., 1995, *Nat*, 377, 600
- Parodi B.R., Saha A., Tammann G.A., Sandage A., 2000, *ApJ*, 540, 634
- Pearce F.R., Couchman H.M.P., 1997, *NewA*, 2, 411
- Peebles P.J.E., 1980, *The Large-Scale Structure of the Universe*, Princeton University Press
- Peebles P.J.E., 1984, *ApJ*, 284, 439
- Press W.H., Schechter P., 1974, *ApJ*, 187, 425
- Regös E., Geller M.J., 1989, *AJ*, 98, 755
- Seljak U., Zaldarriaga M., 1996, *ApJ*, 469, 7
- Schechter P.L., 1980, *AJ*, 85, 801
- Shapley H., 1930, *Harvard Obs. Bull.*, 874, 9
- Silk J., 1974, *ApJ*, 193, 525
- Silk J., 1977, *A&A*, 59, 53
- Small T.A., Ma C., Sargent W.L.W., Hamilton D., 1998, *ApJ*, 492, 45
- Suhhonenko I., Gramann M., 1999, *MNRAS*, 303, 77
- Suhhonenko I., Gramann M., 2002, *MNRAS* submitted, astro-ph:0203166
- Tolman R.C., 1934, *Proc. Nat. Acad. Sci.*, 20, 169
- Tytler D., O'Meara J.M., Suzuki N., Lubin D., 2000, *Phys. Scr.*, 85, 12
- van Haarlem M., van de Weygaert R., 1993, *ApJ*, 418, 544
- Villumsen J.V., Davis M., 1986, *ApJ*, 308, 499
- Zel'dovich Ya. B., 1970, *A&A*, 5, 84
- Yahil A., 1985, In *The Virgo Cluster*, ed. O. Richter & V. Bingelli, ESO, Garching, p. 359